Soil moisture and electrical conductivity relationships under typical Loess Plateau land covers

[1] Tuvia Turkeltaub, [2] Jiao Wang, [1,3] Qinbo Cheng, [2,4] Xiaoxu Jia, [4]Yuanjun Zhu, [2,4] Ming-An Shao and [1]Andrew Binley

[1] Lancaster Environment Centre, Lancaster University, Lancaster, UK, LA1 4YQ, UK.

[2] Key Laboratory of Ecosystem Network Observation and Modeling, Institute of Geographical Sciences and Natural Resources Research, Chinese Academy of Sciences, Beijing 100101, China

[3] State Key Laboratory of Hydrology, Water Resources and Hydraulic Engineering, Hohai University, Nanjing 210098, China

[4] State Key Laboratory of Soil Erosion and Dryland Farming on the Loess Plateau, Northwest A&F University, Yangling 712100, China

* Correspondence: tuviat@bgu.ac.il; Tel.: +972-526-137-442

Abstract

Vegetation changes that are driven by soil conservation measures significantly affect subsurface water flow patterns and soil water status. Much research on water consumption and sustainability of newly introduced vegetation types at the plot scale has been done in the Loess Plateau of China (LPC), typically using local scale measurements of soil water content (SWC). However, information collected at the plot scale cannot readily be up-scaled. Geophysical methods such as electromagnetic induction (EMI) offer large spatial coverage and therefore could bridge between the scales. A non-invasive, multi-coil, frequency domain, EMI instrument was used to measure the apparent soil electrical conductivity (σ_a) from six effective depths under four typical land-covers; shrub, pasture, natural fallow and crop, in the north of the LPC. Concurrently, SWC was monitored to a depth of 4 m depth using an array of 44 neutron probes distributed along the plots. The measurements of σ_a for six effective depths and the integrated SWC over these depths, show consistent behavior. High variability of σ_a under shrub cover, in particular, is consistent with long term variability of SWC, highlighting the potential unsustainability of this land cover. Linear relationships between SWC and σ_a were established using cumulative sensitivity forward models. The conductivity-SWC model parameters show clear variation with depth, despite lack of appreciable textural variation. This is likely related to the combined effect of elevated pore water conductivity as was illustrated by the simulations obtained with water flow and solute transport models. The results of the study highlight the potential for the implementation of the EMI method for investigations of water distribution in the vadose zone of the LPC, and in particular for qualitative mapping of the vulnerability to excessive vegetation demands, and hence unsustainable land cover.

Keywords: land-use change, revegetation, electromagnetic induction, soil moisture, hydrogeophysics

1. Introduction

Landscape alternation as conversion of natural ecosystems to agricultural lands, or application of soil conservation measures as revegetation for preventing land degradation, have a significant impact on soil water dynamics. The conversion of natural vegetation to croplands with shallow rooting systems can increase water levels in unconfined aquifers and mobilizes salts to groundwater (Hancock et al., 2008; Radford et al., 2009; Scanlon et al., 2009; Kurtzman and Scanlon, 2011). Afforestation or revegetation, where trees, grass and shrubs are replanted, were related to depletion of soil water and reduction in groundwater recharge fluxes (Scott and Lesch, 1997; Allen and Chapman, 2001; Zhang et al., 2008; Gates et al., 2011; Huang et al., 2013; Adane et al., 2018; Bai et al., 2020; Ouyang et al., 2021). Various factors are attributed to the disturbance of the soil water status such as high water demand, larger water-holding capacity of forest soils, deep roots, climate variability and plantation of vegetation in an inadequate environment (Cramer et al., 1999; Rodriguez-Iturbe et al., 2001; Jia and Shao, 2014; Barbeta et al., 2015; Lazo et al., 2021). However, the effect on water yield by revegetated areas is debatable and depends on different conditions (van Dijk and Keenan, 2007). Therefore, there is a growing interest in development of monitoring methodologies to improve our knowledge of these processes (Robinson et al., 2008; Krause et al., 2015).

The soil water content (SWC) comprises information regarding the interaction between climate, vegetation and soil (Rodriguez-Iturbe et al., 2001; Vereecken et al., 2014). Nevertheless, SWC is spatially and temporally highly variable (Western et al., 2002). Remote sensing of SWC can provide valuable spatial information of SWC but only on the top few centimeters of the soil; other methods, such as TDR and neutron probes, are limited in their support volume. In contrast, geophysical methods, such as ground penetrating radar, electromagnetic induction (EMI) and electrical resistivity, can be used for monitoring subsurface water and solute dynamics at a range of temporal and spatial scales (Binley et al., 2015).

The link between soil electrical conductivity (σ) and SWC has been the focus of attention for some time. Gardner (1898) first proposed the use of electrical conductivity for inferring SWC. Although σ is strongly influenced by soil water content, it is also affected by other factors, such as soil texture, temperature and pore water electrical conductivity (e.g., Friedman, 2005), necessitating the development of local (site specific) relationships between

σ and SWC. Binley and Slater (2020) provide a comprehensive analysis of the properties and states of soil that influence electrical conductivity. In Section 2 we discuss the relationship between σ and SWC in detail, and in the context of the current study.

The EMI method measures the apparent bulk electrical conductivity of the soil (σ_a), which is the depth weighted average value of the σ, with no requirement to establish any contact with the soil surface. The apparent conductivity is an integrated measurement of electrical conductivity that is governed by the depth-sensitivity pattern of the specific measurement. EMI is a relatively mobile technique allowing the measurement of σ_a over large scales (Abdu et al., 2008; Robinson et al., 2012). Doolittle and Brevik (2014) review the use of EMI measurements for qualitative mapping of soil properties and soil water processes. A number of studies have illustrated the potential and challenges of the EMI method for estimation of SWC over large areas by establishing relationships between σ_a and SWC (Robinson et al., 2012; Nagy et al., 2013; Calamita et al., 2015; Martini et al., 2017; Altdorff et al., 2018; Martínez et al., 2020). Although the σ_a - SWC relationship can indicate the integrated state of the soil water, a detailed description of the soil water state with depth is limited (Corwin and Rhoades 1982; Hendrickx et al., 2002). Modern EMI devices are manufactured with multiple coils and multiple frequencies, enabling the simultaneous measurement of σ_a from multiple effective depths. This permits the inversion of the measured σ_a values in order to obtain the 'real' soil conductivity, σ. Previous studies suggested a number of approaches to establish the σ - SWC relationship under field conditions for different soil types (Huang et al., 2016, 2017). They used σ values derived from inversion of the σ_a data and related these to observed SWC values. The major drawback of the inversion solution is non-uniqueness, i.e. multiple solutions for the same dataset. To encourage unique solutions and reduce some uncertainties, various approaches are suggested such as regularization or joint inversions of geophysical datasets (Constable, 1987; Linde et al., 2006). Recently, Robinet et al. (2018) reported on difficulties to invert σ_a for the establishment of *in situ* σ - SWC relationships. Instead, they utilized a σ_a forward modeling approach to develop field-based σ - SWC relationships.

Given the potential value of EMI for mapping variation in soil water and the need to understand the impact of land management practices, we carried out EMI measurements over four typical land covers (Peashrub, Purple Alfalfa, millet/soybean and fallow) at a study site in the north of the Chinese Loess Plateau. Previous studies have documented long term SWC

observations up to 4 m depth under each of the four plots (Liu and Shao, 2016; Zhao et al., 2017). Liu and Shao (2016) showed that the vegetation type significantly controls the vadose zone water dynamics. Furthermore, Zhao et al. (2017) analyzed a 10 year record of soil water variability under different land covers and revealed high temporal variability (coefficients of variation up to 40% to depths of 4 meters) under Purple Alfalfa and Peashrub covers, which reflect the significant water demands by these vegetation types. Earlier studies (e.g Li et al., 2008) have shown that water uptake under these vegetation types can extend to several meters depth. From the investigation of Zhao et al. (2017), the millet and soybean (and fallow) land covers seem to be the most sustainable in this environment. Therefore, the first objective of this study was to explore the capability of using σ_a, measured by EMI, to assess water sustainability of particular land covers. The second objective was to explore the σ - SWC relationships in the deep vadose zone under the different land covers. Most previous soil water – EMI studies have targeted relatively shallow variation in electrical conductivity; here we study variation in soil water and σ to depths of 4m.

2. Method

2.1 Study Site

This study was conducted at the Shenmu Soil Erosion and Environment Experimental Station (38°47′46″ N, 110°21′55″ E) on the northern LPC. The mean annual air temperature is 8.4 °C, the annual reference evapotranspiration (ET_0) is 1020 mm and the average annual precipitation is 437 mm, 70% of which falls from July through October (climate records are presented in *Supporting Information*). Significant soil erosion driven by wind and rainfall in this region motivated the implementation of a large scale vegetation restoration, the 'Grain to Green' project, to improve soil stability (Jia and Shao, 2014; Feng et al., 2016). Since 1999, many farmlands were converted into forest and grassland, mainly in areas where slopes exceed 15^0 (Liang et al., 2015). Throughout the replantation project, nonindigenous and indigenous vegetation were introduced to the region (Feng et al., 2016). The study site was established to understand the impact of introducing different cover types in the Loess Plateau. Experimental data has indicated that the nonindigenous vegetation appear to have excessive demands on soil water, keeping the soil under dry conditions and limiting soil water replenishment, in addition to reducing aquifer recharge. Therefore, the sustainability of some introduced land cover types is in question (Liu and Shao, 2016; Zhao et al., 2017).

Four adjacent plots (61 m×5 m) were established in 2004 on slopes with a uniform gradient (12–14°) (Figure 1). To test the effect of different vegetation types on the dynamics of soil water, three vegetation covers were introduced: "shrub" (Korshinsk Peashrub - *Caragana korshinskii*); "grass" (Purple Alfalfa - *Medicago sativa*); "crop" (two-year rotation of millet and soybean). A "fallow" plot was also created. This was cultivated until 2004, and subsequently abandoned with no further disturbance. Different vegetation types grow over this plot. For the crop plot, the soybeans/millet were sowed during May and harvested in October. After harvest, the crop plot remains clear of vegetation until following May. Both crops were fertilized with 120 kg ha^{-1} N and 60 kg ha^{-1} P_2O_5 annually, following the recommendation of the local agriculture service. The *Caragana* were planted at a planting spacing of 70 cm×70 cm, then left alone to grow naturally, and alfalfa were planted with a row spacing of 50 cm in 2004. The above-ground parts of the Alfalfa were cut in the beginning of July and October every year. Note that the plots are rainfed and no irrigation is applied. In order to maintain consistency with previous studies at the site, we adopt the same labelling here: shrub (SL), grass (GL), fallow (FL) and crop (CL) (Figure 1).

Neutron-probe access tubes to 4 m depth were installed along 11 points in the centerline of each plot, at 5 m intervals (Figure 1). A previous study (Liu and Shao, 2016) presented analyses of soil samples at the site, indicating similarity in soil physical properties between the plots. The soil is a Calcaric Regosol (FAO-UNESCO), developed from low fertility loess. The soil has weak cohesion, high infiltrability, low water retention, and is prone to erosion (Fu et al., 2010). The soil texture is composed of 11%-14% clay, 30%-45% silt and 45%-51% sand (Liu and Shao, 2016) and can be classified as loam. Figure 2 shows example particle size distribution data from two 3m deep sampling points at the site. The texture profiles show remarkable similarity over 3m depth; from these and other profiles measured at the site, the soil texture spatial variability is insignificant. As part of a regional deep vadose investigation, a borehole was drilled to bedrock at 60 m depth in Shenmu (Jia et al. 2018). Further, observations of bulk density from samples extracted from the deep vadose zone (Figure S2). These observations reveal an increase in bulk density over the top 4m of the profile.

2.2 Data Collection

Soil water content and apparent soil electrical conductivity (σ_a) measurements were carried out during three days in August and September, 2017 (Figure3). All measurements of SWC and σ_a, were conducted at each of the four plots, at the 11 locations in the centerline of each plot. SWC measurements were made using a CNC503DR Hydro probe neutron probe (Beijing Super Power Company, Beijing, China). Neutron counts were taken at an interval of 0.1 m in the upper 1 m and at 0.2 m intervals over 1m to 4 m. Thus in total there are 3300 SWC measurements. Apparent electrical conductivity measurements were made using the CMD Explorer (GF Instruments, Czech Republic) electromagnetic induction (EMI) device, positioned at 1m above ground level and orthogonal to the neutron probe tube. The instrument is 5 m long and has a 10-kHz transmitter coil and three receiver coils at different spacing from the transmitter (1.48m, 2.82m, and 4.49 m). The accuracy of measurement is ±4% at 50 mS/m (GF Instruments, Czech Republic). The instrument is used in two types of coil orientation: horizontal coplanar (HCP) and vertical coplanar (VCP). Thus, the EMI device allows the collection of σ_a from six different effective depths. In total, there are 792 measurements of σ_a. Field tests were conducted to confirm negligible impact of the neutron probe access tube on the measurements when carried out 1m above ground level.

If EMI measurements are made at ground level and assuming relatively uniform electrical conductivity, it is normal practice to assume that the cumulative sensitivity patterns can be expressed, for VCP and HCP orientation, as (McNeill, 1980):

$$CS_{VCP}(z) = \left[4\left(\frac{z}{s}\right)^2 + 1\right]^{0.5} - 2\left(\frac{z}{s}\right) \quad (1)$$

and

$$CS_{HCP}(z) = \left[4\left(\frac{z}{s}\right)^2 + 1\right]^{-0.5} \quad (2)$$

where *s* is the transmitter receiver coil spacing (1.48m, 2.82m or 4.49 m).

In equations (1) and (2) the cumulative sensitivity will be, by definition, unity at the ground surface. As discussed by Morris (2009), measurements made with the coils above ground level result in a modified cumulative sensitivity pattern, as shown in Figure 4 for measurements made 1m above ground level. Adopting, as is common practice for EMI measurements, a definition of the depth of investigation (DOI) as the depth over which 70% of the signal is sensitive to, then for the VCP orientations we can compute a DOI of 2.7m,

212 3.4m and 4.5m for the three-coil spacing, and a DOI of 3.1m, 4.6m, 6.9m for the HCP
213 orientation (see Figure 4).

214

215 **2.3 Establishment of a relationship between SWC and σ**

216 The development of a relationship between SWC and σ is required in order to convert the
217 observed EMI data to SWC. Numerous models have been developed to relate σ to SWC.
218 Many originate from early oil reservoir studies (e.g. the well-established approaches of
219 Archie (1942) and Waxman and Smits (1968)); several approaches have targeted soils (most
220 notably Rhoades et al. (1976)). Models range from purely empirical, semi-empirical to
221 physics-based. Laloy et al. (2011) documents a valuable comparison of a range of models for
222 soils, using the term "pedo-electrical" model to differentiate this from the classical
223 petrophysics terminology.

224 Despite the range of approaches, the general structure of a σ - SWC model is that there
225 should be a conducting term for the pores and a parallel contribution from conduction along
226 the particle surface ('surface conduction'), which is intuitively linked to the proportion of fine
227 particles, often based on clay content (see, for example, Revil and Glover (1998)). Laloy et
228 al. (2011) show, from their comparison, that a volume averaging approach, used by Linde at
229 al.(2006), was the most effective at fitting their experimental data. This model can be written
230 as:

231 $$\sigma = \frac{1}{F}\left[\sigma_f \left(\frac{\theta}{\phi}\right)^n + (F-1)\sigma_s\right], \quad (3)$$

232 where F is the formation factor, σ_f is the fluid electrical conductivity, θ is the SWC, ϕ is
233 porosity, n is a parameter that is controlled by the texture of the media, and σ_s is the surface
234 electrical conductivity. The formation factor, F, is also a function of the soil texture and
235 porosity, typically expressed as ϕ^{-m}, where m is the commonly named cementation
236 exponent.

237 A number of studies have shown that a simple linear relationship can be established between
238 water content and electrical conductivity (e.g., Michot et al., 2003; Calamita et al., 2012;
239 Robinet et al., 2018), which is clearly equivalent to assuming n = 1 in equation (3).
240 Following this, we may write:

$$\sigma = a * \theta + b \quad (4)$$

where, if adopting equation (3), the coefficients are:

$$a = \sigma_f \phi^{m-1},\ b = (1 - \phi^m)\sigma_s\ . \quad (5)$$

To convert the σ from equation 4 to σ_a, the forward solution of the cumulative sensitivity model is utilized, following the approach of Robinet et al. (2018). The EMI instrument measures the bulk apparent electrical conductivity (σ_a), which, using the cumulative sensitivity functions in equations (1) and (2), is related to $\sigma(z)$. Assuming a series of layers, where the middle of each layer is the SWC depth measurement, with conductivity σ_i (i=1,2,3…M), the apparent conductivity for a given coil spacing, s, and orientation, can be expressed as:

$$\sigma_a = \sigma_1[1 - CS(z_1)] + \sum_{i=2}^{M-1} \sigma_i[CS(z_i) - CS(z_{i-1})] + \sigma_M CS(z_{M-1}), \quad (6)$$

where M is the lowest layer. In this study we have SWC observations to 4m depth and so the value of σ_M is assumed to represent the electrical conductivity at greater depths.

The approach adopted involved taking, for all land cover types, measurements of SWC at 25 depths, and converting these to 6 apparent conductivities (3 coil spacings, 2 orientations) for the 11 locations on three dates using a given value of a and b in equation (4). The optimum values of a and b that minimize the root mean square error of a sample size N, given by

$$RMSE = \sqrt{\frac{1}{N}\sum\left(\sigma_{a_{(obs)}} - \sigma_{a_{(predicted)}}\right)^2} \quad (7)$$

where $\sigma_{a_{(obs)}}$ are the observed apparent conductivities and $\sigma_{a_{(predicted)}}$ are the predicted values for a given a and b. The optimization was carried out using the *fminsearch* function that is available on the Matlab optimization toolbox (MathWorks, 2015). This function uses the Nelder-Mead simplex algorithm (Lagarias et al., 1998).

2.4 Unsaturated water flow and solutes transport modelling

For the current study there are no measurements of pore water electrical conductivity. To address this, the Richards equation and the advection – dispersion equation (ADE) were used to simulate the accumulation of chloride in the vadose zone of the four land covers.

We implemented a calibrated unsaturated water flow model that was calibrated to long term data measured at the study site (Bai et al., 2020). For detailed description of the model calibration and validation results, the reader is referred to Bai et al. (2020). The unsaturated water flow is described by the Richards equation:

$$\frac{\partial \theta}{\partial t} = \frac{\partial}{\partial z}\left[K(\psi)\left(\frac{\partial \psi}{\partial z} + 1\right)\right] - S, \quad (8)$$

where ψ is the matric potential head [L], θ is the volumetric water content [$L^3\ L^{-3}$], t is time [T], z is the vertical coordinate [L], K(ψ) [$L\ T^{-1}$] the unsaturated hydraulic conductivity function, is a function of the matric potential head and S is a root water-uptake sink term [$L^3\ L^{-3}\ T^{-1}$]. The Richards equation was solved numerically by using the Hydrus 1D code (Šimůnek et al., 2008). Simulation of the root water uptake rate (the sink term) was conducted according to the model suggested by Feddes et al. (1978); parameters used for the different plant type were obtained from the Hydrus 1D database (millet (crop), grass and alfalfa (shrub)). The Mualem - van Genuchten calibrated unsaturated hydraulic functions obtained by Bai et al. (2020) were implemented in the model.

The ADE was applied to describe the unsaturated chloride transport in the unsaturated zone of the different land covers:

$$\frac{\partial \theta C_{Chloride}}{\partial t} = \frac{\partial}{\partial z}\left[\theta D \frac{\partial \theta C_{Chloride}}{\partial z}\right] - \frac{\partial q C_{Chloride}}{\partial z}, \quad (9)$$

where $C_{Chloride}$ [$M\ L^{-3}$] is chloride concentration in the pore-water solution, D [$L^2\ T^{-1}$] is the hydrodynamic dispersion coefficient and q [$L\ T^{-1}$] is the water flux. Turkeltaub et al. (2018) suggested a representative value of 7.5 cm for the longitudinal dispersivity in the LPC. This value was calculated according to sampled chloride and nitrate vadose zone profiles across the LPC.

Atmospheric boundary conditions with a surface layer (assuming zero for ponding depth at the soil surface) were prescribed at the upper boundary (land surface) as rain, leaf area index (LAI), potential evapotranspiration (ET_0), rain chloride concentrations and the minimum allowed pressure head at the soil surface (hCritA) (Šimůnek et al., 2008) at a daily temporal resolution. To estimate the potential ET_0 values, reference evapotranspiration (ET_{ref}) values were multiplied with the single crop coefficients (Kc). Kc values for millet (crop), grass, alfalfa (shrub) and bare soil were based on Allen et al. (1998). The chloride concentration in the rain was 1.7 mg/L (Huang et al., 2013).

The vertical root density distributions for the different covers were implemented according to the root profiles that were published by Bai et al. (2020). For the crop plot, a linear root distribution was assumed till approximately 50 cm depth (Bai et al., 2021). Under the grass and the shrub plots, the roots were distributed over 400 and 270 cm, respectively (Bai et al., 2021). For the root distribution profiles, the reader is referred to Figure S2 in the supporting information provided by Bai et al. (2020). The increase in leaf area index (LAI) during the growing season for millet, grass and alfalfa was estimated with the model of Leenhardt et al. (1998), where the increase in LAI is assumed a function temperature according to:

$$LAI(T) = \frac{LAI_{max}}{[1+e^{-b(T-T_i)}]}, \qquad (10)$$

where LAI_{max} is the maximum LAI of the crop, T_i (^{0}C) is the sum of temperature at the inflection point of the curve, and b is a curvature parameter. The LAI_{max} and the b parameters were estimated using the temperature database and reported LAI curves (McVicar et al., 2005, natural grass; Wu et al., 2003, millet; Zhao et al., 2004, alfalfa). For further information of the calculated LAI of the different plant types, the reader is referred to Figure S3 in Supporting Information. Daily climate data, covering the period 01-Jan-1961 to 31-Dec-2017, were obtained in the vicinity of the study site (State Bureau of Meteorology, 2020; http://cdc.cma.gov.cn). The simulations started in 01-Jan-1961 and ceased on the 21-Aug-2017 (20718 days). By running the models over a long period, the effect of the initial conditions was minimized. The models performance evaluation was conducted following the analysis suggested by Bai et al. (2020). Three types of statistical measures were used: (1) The Nash-Sutcliffe efficiency coefficient (NSE); (2) root mean square error (RMSE); (3) mean absolute percent error (MAPE). The closer NSE to 1, the better the model fit. Lower values of RMSE and MAPE indicate a better fit between model and data.

3. Results and Discussion

3.1 Spatio-Temporal Variability of SWC

In Figure 5, SWC profiles for all the survey dates are shown. The movement of a drying front can be seen between the first two survey dates, followed by subsequent wetting in the third survey (following the late August rainfall event). The profiles show similarity for a given land cover type (limited horizontal variability was observed along the slope) and also the

reduced soil water content at depth for the grass and shrub cover type, due to the greater water demands of such cover and the deep root penetration, which is estimated to be greater than 4 m depth (Zhao et al. 2017). These are consistent with the long term study at the site of Zhao et al. (2017) who also showed that water percolates to deeper parts of the vadose zone under the crop cover compared to the other land covers. The significant differences in SWC between the land covers, which are subjected to the same climatic conditions, and uniform soil texture (Figure 2), highlights the potential negative effect on SWC due to the plantation of vegetation that is unsustainable in the LPC region (Fang et al., 2016; Liu and Shao, 2016; Zhao et al., 2017). Figure 6 summarizes the SWC data for the three survey dates, adding further illustration of the effect of land cover type on soil water availability.

3.2 σ_a Measurements

The apparent conductivity measurements are summarized as box and whisker plots in Figure 7. The vertical coplanar and horizontal coplanar configurations with similar depths of investigation show consistency. The plots indicate an increasing conductivity with depth across all land cover types and a clear contrast in apparent conductivity for the four land covers, particularly for the measurements over greater depths. There is a clear similarity between land cover contrasts in SWC (Figure 6) and apparent conductivity (Figure 7), particularly when we compare the shrub and grass cover to the fallow and crop cover.

Robinson et al. (2008) reported on similar variability in σ_a for different vegetation species. They related the ranking in σ_a values to the relationship between plant communities and soil types. The plots in the current study are, however, adjacent and major differences in soil texture are not observable (Figure 2). Therefore, it can be assumed that the ranking of σ_a is probably dominated by the water conditions in the vadose zone, influenced by the water demand of the vegetation cover. We note that some discrepancy between crop and fallow cover might be related to the fertilizer application for the crop (Zhao et al., 2017). Similar observations were reported elsewhere (Calamita et al., 2015). Nevertheless, the σ_a values obtained at the crop and fallow are generally higher to those obtained on the shrub and grass plots, which are known to experience bigger demands on soil water status.

Further interpretation was suggested in previous studies regarding the statistics of the σ_a values (Robinson et al., 2008; Calamita et al., 2015). For the following interpretation, two

assumptions are made: 1) the σ_a measurements reflect the soil water conditions (as was shown above) and 2) vegetation under optimal conditions would show a low coefficient of variation (CV) of the SWC (Robinson et al., 2008; Zhao et al., 2017). Robinson et al. (2008) showed empirically that highly skewed σ_a distributions and high CVs values indicate that vegetation grows outside their optimal environment. The long-term investigation (over 10 years) of SWC time series measurements at the study site by Zhao et al. (2017) revealed a decreasing trend in the coefficient of variation of SWC as follows: crop < fallow < grass < shrub. Similarly, a high coefficient of variation was calculated for the σ_a measurements under the shrub cover (Table 1). Thus, following the presented analysis, we observe the same ranking of variation in apparent conductivity for the deeper measurements (see Table 1). Based on their observations of SWC, Zhao et al. (2017) concluded that the Korshinsk Peashurb is not sustainable, in terms of SWC use, in the region. The EMI results presented here may offer a means of detecting areas that might be affected by revegetated plants under unsustainable conditions in the LPC.

3.3 SWC - σ Relationship

The measurements obtained in the current study enabled us to explore relationships between SWC and σ at the study site. As stated earlier, the approach involved compiling an aggregate dataset for the site, rather than applying the model search for different cover types, since there is likely to be a limited range of the data to perform the latter. Table 2 reports the linear coefficients *a* and *b* (equation 4) obtained using the optimization process adopted here. The fit for each model is similar, approximately 1mS/m, which is within the accuracy of the instrument. Power law models were also tested, however, these models did not provide any further improvement in performance, which is in line with previous studies (Michot et al., 2003; Calamita et al., 2012). In addition, Robinet et al. (2018) noted that a better linear relationship between σ_a and soil moisture could be obtained by using σ_a observations from their deeper sensed EMI configuration.

Figure 8 shows the model fit for the six coil orientations, plotted to differentiate the four cover types. The grass and shrub cover data show the greatest departure from the 1:1 apparent conductivity, particularly at greater depths. This may be related to the relatively high salinity conditions that might prevail under these cover types due to elevated evapotranspiration.

Figure 9 shows the variation in σ - SWC relationship parameters with depth, using a nominal depth as that at which the cumulative sensitivity function CS(z) equals 0.5, i.e., the depth over which 50% of the EMI measurement is sensitive to. Note that this 'halfdepth' is a nominal depth, used for illustration, although it is sometimes used to guide EMI survey design (see Morris, 2009). A consistent increase with depth in both a and b is seen for both coil orientations. From equation (5) an increase in a could be accounted for (i) increase in pore water conductivity, (ii) reduction in porosity, (iii) increase in cementation exponent, m. An increase in b can also be attributed to a reduction in porosity and an increase in m, in addition to an increase in surface conductivity. The observations of bulk density reveal an increase in bulk density over the top 4m of the profile (Figure S2). Assuming a particle density of 2.65 g/cm^3, this equates to a reduction in porosity from 0.50 at 0.5m depth to 0.44 at 4.5m depth, i.e. a reduction by 10%. Assuming a cementation exponent, m = 2 since most porous sediments have cementation exponents between 1.5 and 2.5 (Cai et al., 2017) such a reduction in porosity can only account for a 30% increase in a. It would appear, therefore, that pore water conductivity variation with depth is a primary driver of the change in model coefficients with depth.

Developing relationships between soil water content and electrical conductivity is constrained by the influence of a range of properties, making the use of universal models somewhat limited without local calibration. GF Instruments report that the measurement accuracy for the CMD-Explorer is ± 4% and the measurement accuracy of the CNC503DR Hydro neutron probe is also reported to be about 4%. The RMSE values of all the models are 10% or lower than the mean of the measurements. Furthermore, the R^2 and the RMSE values that were reported here are comparable to previously published calibrated models (Tromp-van Meerveld & McDonnell, 2009; Robinson et al., 2012; Calamita et al., 2015; Coppola et al., 2016; Robinet et al., 2018). Therefore, for the dataset studied here a linear σ – SWC model was considered to be suitable. Although we recognize that given a wider range of soil water a more non-linear function may be suitable (as in, for example, Robinet et al., 2018). Despite this, our results show that, qualitative mapping of the impact of soil water reduction from excessive crop water uptake is potentially feasible in the Loess Plateau region of China.

3.4 Accumulation of chloride in the vadose zone

Simulated and observed SWC are plotted in Figure S4 and Figure S5 in the Supporting Information. Note that the soil hydraulic functions and root vertical distributions were prescribed according to Bai et al. (2020) and no further adjustments were conducted. The RMSE and MAPE were similar and low for all the plots (Figure S5), while the NSE value was different for each plot and showed higher efficiency for the Crop and Grass plots (Figure S5). These results were comparable to the analysis presented by Bai et al. (2020). Thus, the model can be considered to adequately describe the SWC dynamic under the investigated plots (Bai et al., 2020). By including the longitudinal dispersivity in the model, the transport of chloride (of rainfall origin) in the vadose zone under the different covers is revealed.

Figure 10 presents the calculated chloride concentrations at the end of the model runs (20th September 2017). The simulated chloride concentrations under the alfalfa are nearly two times higher compared with the fallow and six times that with the crop (millet, Figure 10). Previous studies in the LPC reported soil profile information that are comparable to the simulated chloride. Huang et al. (2013) showed an intensive accumulation of chloride under alfalfa (about 6.5 times higher than under rain-fed winter wheat crop). Additional studies (Gates et al., 2011; Huang et al., 2021) revealed an increase in chloride accumulation in the vadose zone under similar shrub covers as in this study and under orchards in the LPC.

An earlier study by Hilhorst (2000) suggested that under dry conditions, the σ_a measured by EMI, is more affected by the increase of pore water conductivity and less closely associated to SWC. Furthermore, in semi-arid areas the climatic forcing has a major effect on deep drainage. The level of deep drainage intensity would define the build-up of salts and their distribution in vadose zone (Scanlon et al., 2010). Recently, several studies have indicated that the pore-water conductivity distribution in the vadose zone should be considered when establishing an *in situ* σ - SWC relationship in semi-arid areas (Moreno et al., 2015; Cassiani et al., 2016). However, currently there are no reported field studies of *in situ* simultaneous measurements of SWC, σ_a and pore water conductivity under semi-arid conditions. The build-up of salts and associated soil salinity in the LPC vadose zone has surprisingly received little attention.

4. Summary and Conclusions

452 The measurements of SWC in deeper parts of the vadose zone at large scales is challenging.
453 Geophysical methods such as the EMI approach might facilitate a bridge between processes
454 observed locally and at larger scales. Here, EMI was applied to measure apparent electrical
455 conductivity over six effective depths in four plots covered by typical land cover types
456 (shrub, grass, fallow and crop) in the north of the LPC. SWC were measured with neutron
457 probes from the ground surface to a depth of 4 meters. The unique loess environment in the
458 LPC, with its characteristic deep soils and relatively insignificant soil variability, reduces the
459 effect of soil texture variation on EMI readings to minimum. Moreover, for this particular
460 study, soil textural variation is insignificant and can be neglected. The similarity of the soil
461 texture between all plots enabled a focus of investigation on the potential influences of
462 different cover types on the spatiotemporal variability of SWC and apparent electrical
463 conductivity.

464 An increasing trend in σ_a values: SL<GL<FL<CL, corresponds with the increase in average
465 SWC in the plots. Moreover, σ_a values that were measured in the shrub covered plot show a
466 relatively high variability, which is consistent with documented variability of SWC for soils
467 under this vegetation, indicating unsustainable water conditions in the vadose zone.

468 Linear relationships between soil water content and specific-depth soil electrical conductivity
469 (σ) under the different land covers were established. The σ values were estimated using the
470 SWC observations, assuming a linear relationship between these variables. The analysis
471 reveals a change in model parameters with depth. Textural variation is apparently negligible
472 (to 3m depth at least), however, such variation in model parameters may be attributed, in part,
473 to changes in bulk density. Increases in pore water electrical conductivity are hypothesized as
474 a primary cause of the depth dependency of the σ - SWC model parameters. Simulations of
475 chloride profiles support the hypothesis that contrasts in pore water electrical conductivity
476 could exist under different crop types. Elevated pore water conductivity beneath shrub and
477 grass covers would imply even greater significance of the soil water content since these two
478 cover types exhibit lower apparent conductivity than the other two cover types. To improve
479 SWC prediction from EMI observations pore-water conductivity should be measured.
480 Nevertheless, the results presented here illustrate how excessive water demands of Korshinsk
481 Peashrub and Purple Alfalfa at the study site are revealed by their lower apparent
482 conductivity and (for the case of the shrub cover at least) their high variation in apparent
483 conductivity. Our EMI dataset reveals an immense potential for mapping, qualitatively at

484 least, areas of the Loess Plateau that are vulnerable to excessive vegetation demands, and
485 hence unsustainable land cover.

486

487 **Acknowledgments**

488 This work was supported by the UK Natural Environment Research Council (grant ref
489 NE/N007409/1 awarded to Lancaster) and the National Natural Science Foundation of China
490 (41571130081). We appreciate Dr. Yuanzhi Wu from Linyi University for her generosity in
491 providing the particle size distribution data.

492

493 **References**

494 Allen, R. G., Pereira, L. S., Raes, D., & Smith, M. (1998). Crop evapotranspiration:
495 Guidelines for computing crop water requirements, FAO Irrigation and Drainage Pap. 56,
496 Food and Agric. Organ of the U. N., Rome.

497 Abdu, H., Robinson, D.A., Seyfried, M. & Jones, S.B. (2008). Geophysical imaging of
498 watershed subsurface patterns and prediction of soil texture and water holding capacity.
499 *Water Resources Research*, 44, W00D18. http://doi.org/10.1029/2008WR007043.

500 Adane, Z.A., Nasta, P., Zlotnik, V., & Wedin, D. (2018). Impact of grassland conversion to
501 forest on groundwater recharge in the Nebraska Sand Hills. *Journal of Hydrology:*
502 *Regional Studies*, 15, 171–183. https://doi.org/10.1016/j.ejrh.2018.01.001.

503 Allen, A., & Chapman, D. (2001). Impacts of afforestation on groundwater resources and
504 quality. *Hydrogeology Journal*, 9, 390-400. https://doi.org/10.1007/s100400100148.

505 Altdorff, D., Galagedara, L., Nadeem, M., Cheema, M., & Unc, A. (2018). Effect of
506 agronomic treatments on the accuracy of soil moisture mapping by electromagnetic
507 induction. *Catena*, 164, 96-106. https://doi.org/10.1016/j.catena.2017.12.036.

508 Archie, G.E. (1942). The electrical resistivity log as an aid in determining some reservoir
509 characteristics. *Transactions of the American Institute of Mining, Metallurgical, and*
510 *Petroleum Engineers,* 146, 54–62. http://dx.doi.org/10.2118/942054-G.

511 Bai, X., Jia, X., Jia, Y., & Hu, W. (2020). Modeling long-term soil water dynamics in
512 response to land-use change in a semi-arid area. *Journal of Hydrology*, 585, 124824.
513 http://dx.doi.org/10.1016/j.jhydrol.2020.124824

514 Barbeta, A., Mejía‐Chang, M., Ogaya, R., Voltas, J., Dawson, T.E., & Peñuelas, J. (2015).
515 The combined effects of a long‐term experimental drought and an extreme drought on
516 the use of plant‐water sources in a Mediterranean forest. *Global change biology*, 21,
517 1213-1225. https://doi.org/10.1111/gcb.12785.

518 Binley, A. & Slater, L. (2020). *Resistivity and Induced Polarization. Theory and*
519 *Applications to the Near-Surface Earth*, Cambridge University Press, 388pp.

520 Binley, A., Hubbard, S.S., Huisman, J.A., Revil, A., Robinson, D.A., Singha, K. & Slater,
521 L.D. (2015). The emergence of hydrogeophysics for improved understanding of
522 subsurface processes over multiple scales. *Water Resources Research*, 51(6), 3837-3866.
523 https://doi.org/10.1002/2015WR017016.

524 Cai, J., Wei, W., Hu, X., & Wood, D. A. (2017). Electrical conductivity models in saturated
525 porous media: A review. *Earth-Science Reviews*, 171, 419-433.
526 https://doi.org/10.1016/j.earscirev.2017.06.013.

527 Calamita, G., Brocca, L., Perrone, A., Piscitelli, S., Lapenna, V., Melone, F., & Moramarco,
528 T. (2012). Electrical resistivity and TDR methods for soil moisture estimation in central
529 Italy test-sites. *Journal of Hydrology*, 454, 101-112.
530 https://doi.org/10.1016/j.jhydrol.2012.06.001.

531 Calamita, G., Perrone, A., Brocca, L., Onorati, B., & Manfreda, S. (2015). Field test of a
532 multi-frequency electromagnetic induction sensor for soil moisture monitoring in
533 southern Italy test sites. *Journal of Hydrology*, 529, 316-329.
534 https://doi.org/10.1016/j.jhydrol.2015.07.023.

535 Canadell J., R.B. Jackson, J.R. Ehleringer, H.A. Mooney, O.E. Sala, & Schulze, E. D. (1996).
536 Maximum rooting depth of vegetation types at the global scale. *Oecologia*, 108, 583– 595.

537 Cassiani, G., Boaga, J., Rossi, M., Putti, M., Fadda, G., Majone, B., & Bellin, A. (2016).
538 Soil–plant interaction monitoring: small scale example of an apple orchard in Trentino,

539 North-eastern Italy. *Science of the Total Environnent*, 543, 851-861.
540 https://doi.org/10.1016/j.scitotenv.2015.03.113.

541 Corwin, D.L., & Rhoades, J.D. (1982). An improved technique for determining soil electrical
542 conductivity — depth relations from above-ground electromagnetic measurements. *Soil*
543 *Science Society of America Journal*, 46, 288–291.
544 https://doi.org/10.2136/sssaj1982.03615995004600030014x.

545 Constable, S.C. (1987). Occam's inversion: A practical algorithm for generating smooth
546 models from electromagnetic sounding data. *Geophysics*, 52, 289–
547 300.https://doi.org/10.1190/1.1442303

548 Coppola, A., Smettem, K., Ajeel, A., Saeed, A., Dragonetti, G., Comegna, A., Lamaddalena,
549 N. & Vacca, A. (2016). Calibration of an electromagnetic induction sensor with time-
550 domain reflectometry data to monitor rootzone electrical conductivity under saline water
551 irrigation. European Journal of Soil Science, 67(6), 737-748.
552 https://doi.org/10.1111/ejss.12390.

553 Cramer, V. A., Thorburn, P. J., & Fraser, G. W. (1999). Transpiration and groundwater
554 uptake from farm forest plots of Casuarina glauca and Eucalyptus camaldulensis in saline
555 areas of southeast Queensland, Australia. *Agricultural Water Management*, 39, 187–204.
556 https://doi.org/10.1016/S0378-3774(98)00078-X.

557 Doolittle, J. A., & Brevik, E. C. (2014). The use of electromagnetic induction techniques in
558 soils studies. *Geoderma*, 223, 33-45. https://doi.org/10.1016/j.geoderma.2014.01.027

559 Fan, J., Wang, Q., Jones S. B., & Shao M. (2016). Soil water depletion and recharge under
560 different land cover in China's Loess Plateau. *Ecohydrology*, 9, 396–406.
561 https://doi.org/10.1002/eco.1642.

562 Fang, X.N., Zhao,W.W., Wang, L.X., Feng, Q., Ding, J.Y., Liu, Y.X., & Zhang, X. (2016).
563 Variations of deep soil moisture under different vegetation types and influencing factors
564 in awatershed of the Loess Plateau, China. *Hydrology and Earth System Sciences*, 20,
565 3309–3323. https://doi.org/10.5194/hess-20-3309-2016

566 Feddes, R.A., Kowalik, P.J., & Zaradny, H. (1978). Simulation of field water use and crop
567 yield. John Wiley and Sons, New York.

568 Feng, X., et al. (2016). Revegetation in China's Loess Plateau is approaching sustainable
569 water resource limits. Nature Climate Change, 6.
570 http://dx.doi.org/10.1038/NCLIMATE3092.

571 Friedman, S.P. (2005). Soil properties influencing apparent electrical conductivity: a review.
572 *Computers and Electronics in Agriculture*, 46, 45–70.
573 https://doi.org/10.1016/j.compag.2004.11.001.

574 Fu, X., Shao, M., Wei, X., & Horton, R. (2010). Soil organic carbon and total nitrogen as
575 affected by vegetation types in Northern Loess Plateau of China. *Geoderma*, 155(1-2),
576 31-35. https://doi.org/10.1016/j.geoderma.2009.11.020.

577 Gardner, F. D. (1898). The electrical method of moisture determination in soils: results and
578 modifications in 1987, U. S. Dept. Agri. Div. of Soils Bull., No. 12.

579 Garré, S., Coteur, I, Wongleecharoen, C., Kongkaew, T., Diels, J., & Vanderborght, J.
580 (2013). Noninvasive monitoring of soil water dynamics inmixed cropping systems: a case
581 study in Ratchaburi Province, Thailand. *Vadose Zone Journal*, 12 (2).
582 https://doi.org/10.2136/vzj2012.0129.

583 Gates, J.B., Scanlon, B.R., Mu, X., & Zhang, L. (2011). Impacts of soil conservation on
584 groundwater recharge in the semi-arid Loess Plateau, China. *Hydrogeology Journal*, 19,
585 865–875. https://doi.org/10.1007/s10040-011-0716-3.

586 Hancock, T.C., Sandstrom, M.W., Vogel, J.R., Webb, R.M.T., Bayless, E.R., & Barbash, J.E.
587 (2008). Pesticide fate and transport throughout unsaturated zones in five agricultural
588 settings, USA. *Journal of Environmental Quality*, 37, 1086–1100.
589 https://doi.org/10.2134/jeq2007.0024.

590 Hendrickx, J.M.H., Borchers, B., Corwin, D.L., Lesch, S.M., Hilgendorf, A.C., & Schlue, J.
591 (2002). Inversion of soil conductivity profiles from electromagnetic induction
592 measurements: theory and experimental verification. *Soil Science Society of America*
593 *Journal*, 66, 673–685. https://doi.org/10.2136/sssaj2002.6730.

594 Hilhorst, M.A. (2000). A pore water conductivity sensor. *Soil Science Society of America*
595 *Journal*, 64, 1922–1925. https://doi.org/10.2136/sssaj2000.6461922x.

596 Huang, T., Pang, Z., & Edmunds, W.M. (2013). Soil profile evolution following land-use
597 change: implications for groundwater quantity and quality. *Hydrological Process*, 27(8),
598 1238–1252. http://doi.org/10.1002/hyp.9302.

599 Huang, J., Monteiro Santos, F. A., & Triantafilis, J. (2016). Mapping soil water dynamics and
600 a moving wetting front by spatiotemporal inversion of electromagnetic induction data.
601 *Water Resources Research*, 52(11), 9131-9145. http://doi.org/10.1002/2016WR019330.

602 Huang, J., McBratney, A. B., Minasny, B., & Triantafilis, J. (2017). Monitoring and
603 modelling soil water dynamics using electromagnetic conductivity imaging and the
604 ensemble Kalman filter. *Geoderma*, 285, 76-93.
605 https://doi.org/10.1016/j.geoderma.2016.09.027.

606 Huang, Y., Li, B., & Li, Z. (2021). Conversion of degraded farmlands to orchards decreases
607 groundwater recharge rates and nitrate gains in the thick loess deposits. *Science of the*
608 *Total Environment*, 314, 107410. https://doi.org/10.1016/j.agee.2021.107410

609 Jia, Y.H., & Shao, M.A. (2014). Dynamics of deep soil moisture in response to vegetational
610 restoration on the Loess Plateau of China. *Journal of Hydrology*, 519, 523-531.
611 https://doi.org/10.1016/j.jhydrol.2014.07.043.

612 Jia, X., Zhu, Y., Huang, L., Wei, X., Fang, Y., Wu, L., Binley, A., & Shao, M. (2018).
613 Mineral N stock and nitrate accumulation in the 50 to 200 m profile on the Loess Plateau.
614 *Science of the Total Environment*, 633, 999-1006.
615 https://doi.org/10.1016/j.scitotenv.2018.03.249.

616 Lagarias, J. C., Reeds, J. A., Wright, M. H., & Wright, P. E. (1998). Convergence Properties
617 of the Nelder-Mead Simplex Method in Low Dimensions. *SIAM Journal on Optimization*,
618 9, 112–147. https://doi.org/10.1137/S1052623496303470.

619 Leenhardt, D., Lafolie, F., & Bruckler, L. (1998). Evaluating irrigation strategies for lettuce
620 by simulation: 1. Water flow simulations. *European Journal of Agronomy*, 8, 249–265.
621 https://doi.org/10.1016/S1161-0301(97)00065-8

622 Li, J., Chen, B., Li, X.F., Zhao, Y.J., Ciren, Y.J., Jiang, B., Hu, W., Cheng, J.M., & Shao,
623 M.A. (2008). Effects of deep soil desiccation on artificial forestlands in different
624 vegetation zones on the Loess Plateau of China. *Acta Ecologica Sinica*, 28 (4), 1429–
625 1445. https://doi.org/10.1016/S1872-2032(08)60052-9.

626 Li, Z., Chen, X., Liu, W., & Si, B. (2017). Determination of groundwater recharge
627 mechanism in the deep loessial unsaturated zone by environmental tracers. *Science of the*
628 *Total Environment*, 586, 827–835. https://doi.org/10.1016/j.scitotenv.2017.02.061

629 Liang, W., Bai, D., Wang, F., Fu, B., Yan, J., Wang, S., Yang, Y., Long, D., & Feng, M.
630 (2015). Quantifying the impacts of climate change and ecological restoration on
631 streamflow changes based on a Budyko hydrological model in China's Loess Plateau.
632 *Water Resources Research*, 51 (8), 6500–6519. https://doi.org/10.1002/2014WR016589

633 Linde, N., Binley, A., Tryggvason, A., Pedersen, L.B., & Revil, A. (2006). Improved hydro-
634 geophysical characterization using joint inversion of cross-hole electrical resistanceand
635 ground-penetrating radar traveltime data. *Water Resources Research*, 42 (12), 1–
636 16.W12404. https://doi.org/10.1029/2006WR005131.

637 Kurtzman, D., & Scanlon, B.R. (2011). Groundwater recharge through vertisols: Irrigated
638 cropland vs. natural land, Israel. *Vadose Zone Journal*, 10, 662–674.
639 https://doi.org/10.2136/vzj2010.0109.

640 Krause, S., Lewandowski, J., Dahm, C. N., & Tockner, K. (2015). Frontiers in real‐time
641 ecohydrology–a paradigm shift in understanding complex environmental systems.
642 *Ecohydrology* 8, 4, 529-537. https://doi.org/10.1002/eco.1646

643 Laloy, E., Javaux, M., Vanclooster, M., Roisin, C., & Bielders, C. L., (2011). Electrical
644 resistivity in a loamy soil: Identification of the appropriate pedo-electrical model. *Vadose*
645 *Zone Journal*, 10(3), 1023-1033. https://doi.org/10.2136/vzj2010.0095.

646 Lazo, P. X., Mosquera, G. M., McDonnell, J. J., & Crespo, P. (2019). The role of vegetation,
647 soils, and precipitation on water storage and hydrological services in Andean Páramo
648 catchments. *Journal of Hydrology*, 572, 805–819.
649 https://doi.org/10.1016/j.jhydrol.2019.03.050

650 Linde, N., Binley, A., Tryggvason, A., Petersen, L.B., & Revil, A. (2006). Improved
651 hydrogeophysical characterization using joint inversion of cross-hole electrical resistance
652 and ground-penetrating radar traveltime data. *Water Resources Research*, 42, W12404.
653 http://dx.doi.org/10.1029/2006WR005131.

654 Liu, B.X., & Shao, M.A. (2016). Response of soil water dynamics to precipitation years
655 under different vegetation types on the northern Loess Plateau, China. *Journal of Arid*
656 *Land,* 8, 47–59. https://doi.org/10.1007/s40333-015-0088-y.

657 MathWorks (2015). MATLAB. The MathWorks, Inc., Natick, Massachusetts, United States,
658 pp. 2015a.

659 Martini, E., Werban, U., Zacharias, S., Pohle, M., Dietrich, P., & Wollschläger, U. (2017).
660 Repeated electromagnetic induction measurements for mapping soil moisture at the field
661 scale: validation with data from a wireless soil moisture monitoring network. *Hydrology*
662 *and Earth System Sciences*, 21 (1), 495–513. https://doi.org/10.5194/hess-21-495-2017.

663 Martínez, G., Laguna, A.M., Giráldez, J.V., & Vanderlinden, K. (2020). Concurrent
664 variability of soil moisture and apparent electrical conductivity in the proximity of olive
665 trees. *Agricultural Water Management*, 245, 106652.
666 https://doi.org/10.1016/j.agwat.2020.106652.

667 McNeill, J.D. (1980). Electromagnetic terrain conductivity measurement at low induction
668 numbers. Technical Note TN-6. Geonics Ltd., Mississauga, Ont., Canada.

669 McVicar, T. R., Li, L. T., Van Niel, T. G., Hutchinson, M. F., Mu, X. M., & Liu, Z. H.
670 (2005). Spatially distributing 21 years of monthly hydrometeorological data in China:
671 Spatio-temporal analysis of FAO-56 crop reference evapotranspiration and pan evaporation
672 in the context of climate change. Land and Water Tech. Rep. 8/05, *Commonw. Sci. and Ind.*
673 *Res. Org.*, Canberra, ACT, Australia.
674 http://www.clw.csiro.au/publications/technical2005/tr8-05.pdf.

675 Michot, D., Benderitter, Y., Dorigny, A., Nicoullaud, B., King, D., & Tabbagh, A. (2003).
676 Spatial and temporal monitoring of soil water content with an irrigated corn crop cover
677 using surface electrical resistivity tomography. *Water Resources Research*, 39, 1138,
678 https://doi.org/10.1029/2002WR001581.

679 Moreno, Z., Arnon-Zur, A., & Furman, A. (2015). Hydro-geophysical monitoring of orchard
680 root zone dynamics in semi-arid region. *Irrigation Science*, 33(4), 303-318.
681 https://doi.org/10.1007/s00271-015-0467-3.

682 Morris, E.R. (2009). Height above ground effects on penetration depth and response of
683 electromagnetic induction soil conductivity meters. *Computers and Electronics in*
684 *Agriculture,* 68, 150–156. https://doi.org/10.1016/j.compag.2009.05.009

685 Nagy, V., Milics, G., Smuk, N., Kovács, A.J., Balla, I., Jolánkai, M., Deákvári, J., Szalay,
686 K.D., Fenyvesi, L., Štekauerová, V., & Wilhelm, Z. (2013). Continuous field soil
687 moisture content mapping by means of apparent electrical conductivity (ECa)
688 measurement. *Journal of Hydrology and Hydromechanics*, 61, 305–312.
689 https://doi.org/10.2478/johh-2013-0039.

690 Ouyanga, Y., J., Wei, T.D., Leiningerc , Fengd, G., Yange, J. (2021). Impacts of afforestation
691 on groundwater resource: a case study for Upper Yazoo River watershed, Mississippi,
692 USA. Hydrol. Sci. J., 66, 464-473. https://doi.org/10.1080/02626667.2021.1876235.

693 Radford, B.J., D.M. Silburn, & Forster., B.A. (2009). Soil chloride and deep drainage
694 responses to land clearing for cropping at seven sites in Central Queensland, Northern
695 Australia. *Journal of Hydrology*, 379, 20–29.
696 https://doi.org/10.1016/j.jhydrol.2009.09.040.

697 Revil, A., & Glover, P. W. J. (1998). Nature of surface electrical conductivity in natural
698 sands, sandstones, and clays. Geophysical Research Letters, 25(5), 691-694.
699 https://doi.org/10.1029/98GL00296

700 Rhoades, J.D., Raats, P.A.C., & Prather, R.J. (1976). Effects of liquid-phase electrical
701 conductivity, water content, and surface conductivity on bulk soil electrical conductivity.
702 *Soil Science Society of America Journal*, 40, 651–655.
703 http://doi.org/10.2136/sssaj1976.03615995004000050017x.

704 Robinson, D. A., Abdu H., Jones S. B., Seyfried M., Lebron I., & Knight R. (2008). Eco-
705 geophysical imaging of watershed-scale soil patterns links with plant community spatial
706 patterns. *Vadose Zone Journal*, 7(4), 1132–1138. http://doi.org/10.2136/vzj2008.0101.

707 Robinson, D.A., Abdu, H., Lebron, I., & Jones, S.B. (2012). Imaging of hill-slope soil
708 moisture wetting patterns in a semi-arid oak savanna catchment using time-lapse
709 electromagnetic induction. *Journal of Hydrology*, 416, 39-49.
710 https://doi.org/10.1016/j.jhydrol.2011.11.034.

711 Robinet, J., von Hebel, C., Govers, G., van der Kruk, J., Minella, J.P., Schlesner, A.,
712 Ameijeiras-Mariño, Y., & Vanderborght, J. (2018). Spatial variability of soil water
713 content and soil electrical conductivity across scales derived from Electromagnetic
714 Induction and Time Domain Reflectometry. *Geoderma*, 314, 60-174.
715 https://doi.org/10.1016/j.geoderma.2017.10.045.

716 Rodriguez-Iturbe, I., Porporato, A., Laio, F., & Ridolfi, L. (2001). Plants in water-controlled
717 ecosystems: active role in hydrologic processes and response to water stress: I. Scope and
718 general outline. *Advance in Water Research*, 24, 695-705. https://doi.org/10.1016/S0309-
719 1708(01)00004-5.

720 Scanlon, B.R., Stonestrom, D.A., Reedy, R.C., Leaney, F.W., Gates, J.B., & Cresswell, R.G.
721 (2009). Inventories and mobilization of unsaturated zone sulfate, fluoride, and chloride
722 related to land use change in semiarid regions, southwestern United States and Australia.
723 *Water Resources Research*, 45, 1–17. https://doi.org/10.1029/2008WR006963.

724 Scanlon, B.R., Reedy, R.C., Gates, J.B., & Gowda, P.H. (2010). Impact of agroecosystems on
725 groundwater resources in the Central High Plains, USA. *Agriculture, Ecosystems &*
726 *Environment*, 139,700–713. https://doi.org/10.1016/j.agee.2010.10.017.

727 Scott, D. F., & Lesch, W. (1997). Streamflow responses to afforestation with Eucalyptus
728 grandis and Pinus patula and to felling in the Mokobulaan experimental catchments,
729 South Africa. *Journal of Hydrology*, 199, 360-377. https://doi.org/10.1016/S0022-
730 1694(96)03336-7.

731 Šimůnek, J., Šejna, M., Saito, H., Sakai, M., & van Genuchten, M.Th. (2008). The
732 HYDRUS- 1D Software Package for Simulating the Movement of Water, Heat, and
733 Multiple Solutes in Variably Saturated Media. Version 4.0. HYDRUS Software Series 3.
734 Dep. Environmental Sciences, Univ. Calif. Riverside, Riverside, CA.

735 Tromp-van Meerveld, H. J., & McDonnell, J. J. (2009). Assessment of multi-frequency
736 electromagnetic induction for determining soil moisture patterns at the hillslope scale.
737 *Journal of Hydrology*, 368(1-4), 56-67. https://doi.org/10.1016/j.jhydrol.2009.01.037.

738 Turkeltaub, T., Jia, X., Zhu, Y., Shao, M. A., & Binley, A. (2018). Recharge and Nitrate
739 Transport Through the Deep Vadose Zone of the Loess Plateau: A Regional-Scale Model

740 Investigation. *Water Resources Research*, 54(7), 4332-4346.
741 https://doi.org/10.1029/2017WR022190.

742 Turkeltaub, T., Jia, X., Zhu, Y., Shao, M. A., Binley, A., 2021. A Comparative Study of
743 Conceptual Model Complexity to Describe Water Flow and Nitrate Transport in Deep
744 Unsaturated Loess. *Water Resources Research*, 57, e2020WR029250,
745 https://doi.org/10.1029/2020WR029250.

746 van Dijk, A.I.J.M., & Keenan, R.J. (2007). Planted forests and water in perspective. *Forest*
747 *Ecology and Management*, 251 (1–2), 1–9. https://doi.org/10.1016/j.foreco.2007.06.010.

748 Vereecken, H., Huisman, J.A., Pachepsky, Y., Montzka, C., Van Der Kruk, J., Bogena, H.,
749 Weihermüller, L., Herbst, M., Martinez, G., & Vanderborght, J. (2014). On the spatio-
750 temporal dynamics of soil moisture at the field scale. *Journal of Hydrology*, 516, 76-96.
751 https://doi.org/10.1016/j.jhydrol.2013.11.061.

752 Vrugt, J. A., Van Wijk, M. T., Hopmans, J. W., & Simunek, J. (2001). One-, two-, and three-
753 dimensional root water uptake functions for transient modeling. *Water Resources Research*,
754 37, 2457–2470. https://doi.org/10.1029/2000WR000027.

755 Waxman, M.H., & Smits, L.J.M. (1968). Electrical conductivities in oil-bearing shaly sands.
756 *Society of Petroleum Engineers Journal*, 8, 107–122. http://doi.org/10.2118/1863-A.

757 Western, A. W., Grayson, R. B., & Blöschl, G. (2002). Scaling of soil moisture: A hydrologic
758 perspective. *Annual Review of Earth and Planetary Sciences*, 30, 149-180.
759 https://doi.org/10.1146/annurev.earth.30.091201.140434

760 Wu, Y., Xie, K., Zhang, Q., Zhang, Y., Xie, Y., Zhang, G., Zhang, W., & Ritsema, C.J.
761 (2003). Crop characteristics and their temporalchange on the Loess Plateau of China.
762 *Catena*, 54, 7–16. https://doi.org/10.1016/S0341-8162(03)00053-5.

763 Zhang, X., Zhang, L., Zhao, J., Rustomji, P., & Hairsine, P. (2008). Responses of streamflow
764 to changes in climate and land use/cover in the Loess Plateau, China. *Water Resources*
765 *Research*, 44, W00A07. https://doi.org/10.1029/2007WR006711.

766 Zhao, C., Jia, X., Zhu, Y., & Shao, M. A. (2017). Long-term temporal variations of soil water
767 content under different vegetation types in the Loess Plateau, China. *Catena*, 158, 55-62.
768 https://doi.org/10.1016/j.catena.2017.06.006.

769 Zhao, C., Feng, Z., & Chen, G. (2004). Soil water balance simulation of alfalfa (Medicago
770 sativa L.) in the semiarid Chinese Loess Plateau. *Agricultural Water Management*, 69,
771 101–114. https://doi.org/10.1016/j.agwat.2004.04.006

772

773

774

775

776

777

778

779 **Figures**

780 **Figure 1** *Layout of the four plots in the Shenmu Research site. The lower part of the*
781 *photograph is downslope. The black dots in the schematic show the locations of neutron*
782 *probe and EMI measurements.*

783 **Figure 2** *Profiles of particle size distribution for two locations at the site, showing little*
784 *spatial variability in textural properties. The locations of the shrub and fallow plots are*
785 *shown in Figure 1.*

786 **Figure 3** *Daily rainfall between July 2017 and October 2017. The arrows indicate when the*
787 *SWC and EMI surveys were conducted.*

788 **Figure 4** *Cumulative sensitivity functions for vertical coplanar (VCP) and horizontal*
789 *coplanar (HCP) orientations with instrument located 1m above ground level. Arrows are*
790 *positioned at the depth of investigation for a given coil spacing, s.*

791 **Figure 5** *Soil water content profiles in the four plots on the three survey dates. The solid line*
792 *is the median profile; the shaded region shows the 1st and 3rd interquartile range.*

793 **Figure 6** *The average soil water contents under the different land covers. The horizontal line*
794 *shows the median SWC, the box shows the 2nd and 3rd quartile range and the whiskers show*
795 *the 1st and 4th quartiles.*

796 **Figure 7** *Box and whisker plots of the apparent electrical conductivity (σ_a) measurements*
797 *from six effective depths, which were obtained over the different land covers. The horizontal*
798 *line shows the median SWC, the box shows the 2nd and 3rd quartile range and the whiskers*
799 *show the 1st and 4th quartiles.*

800 **Figure 8** *Estimated versus observed σ_a for all crop cover types using the relationships in*
801 *Table 2. The black line in each plot is the 1:1 relationship.*

802 **Figure 9** *Variation in σ - SWC relationship parameters with depth.*

803 **Figure 10** *Simulated chloride profiles in the vadose zone under the four land cover types.*

804

805

806 **Tables**

807 **Table 1.** *Coefficient of variation of apparent conductivity measurements*

Coil configuration and spacing	Crop	Fallow	Grass	Shrub
VCP 1.48m	9.23	15.65	8.57	18.25
VCP 2.82m	8.24	6.30	6.90	13.72
VCP 4.49m	5.45	5.96	7.23	9.98
HCP 1.48m	6.70	5.81	8.90	19.05
HCP 2.82m	6.16	6.23	7.80	12.11
HCP 4.49m	6.84	7.25	8.54	10.68

808

809 **Table 2.** *Estimated relationships between soil water contents and σ for all land covers.*

Configuration	Coil spacing, *s* (m)	DOI (m)	*a* (mS/m)	*b* (mS/m)	RMSE (mS/m)
VCP	1.48	2.7	23.7	1.7	0.7
VCP	2.82	3.4	32.3	4.1	0.8
VCP	4.49	4.5	38.9	5.7	1.0
HCP	1.48	3.1	19.6	5.2	0.8
HCP	2.82	4.6	30.3	7.8	1.0
HCP	4.49	6.9	37.5	9.2	1.3

810

811

812 **Figure 1**

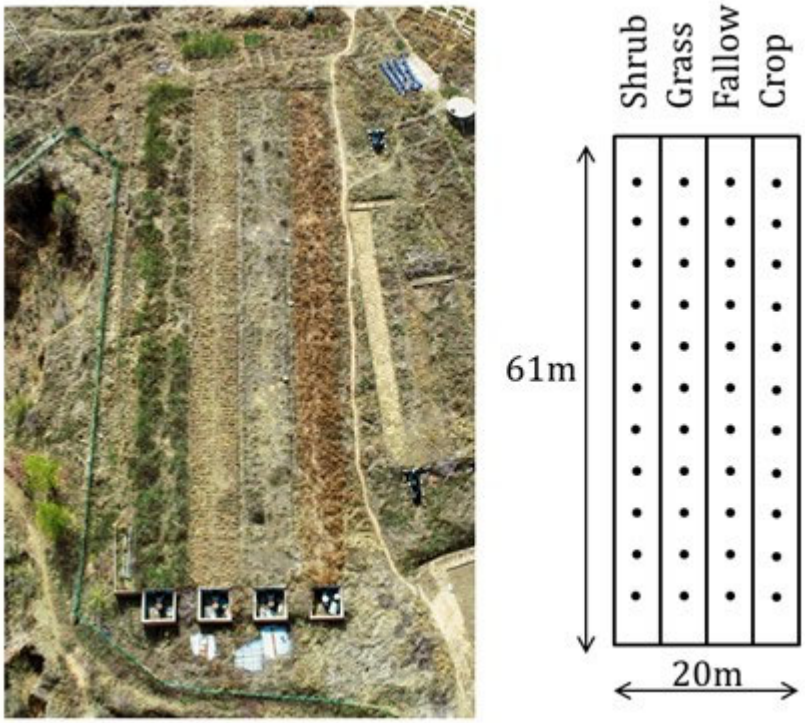

813

814

815

816 **Figure 2**

817

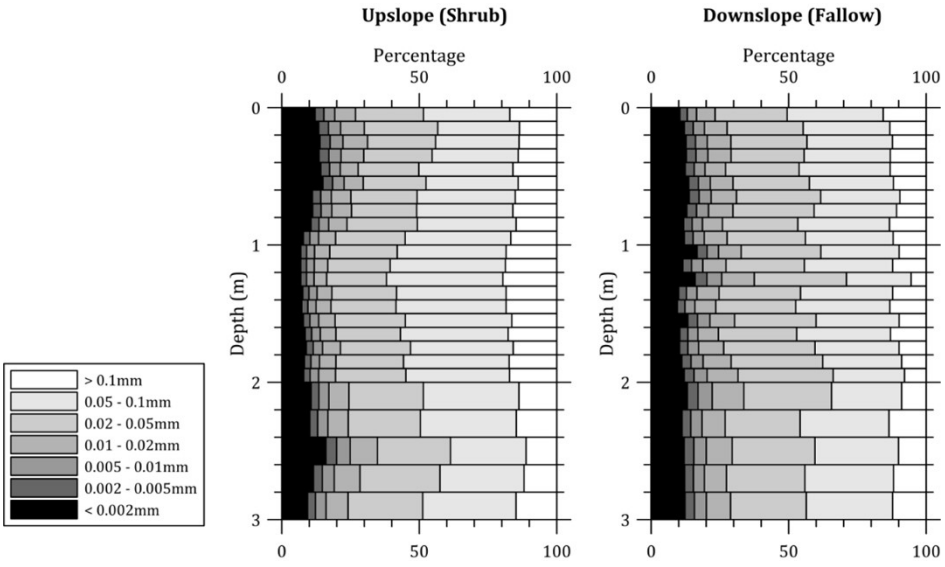

818

819

820

821

822

Figure 3

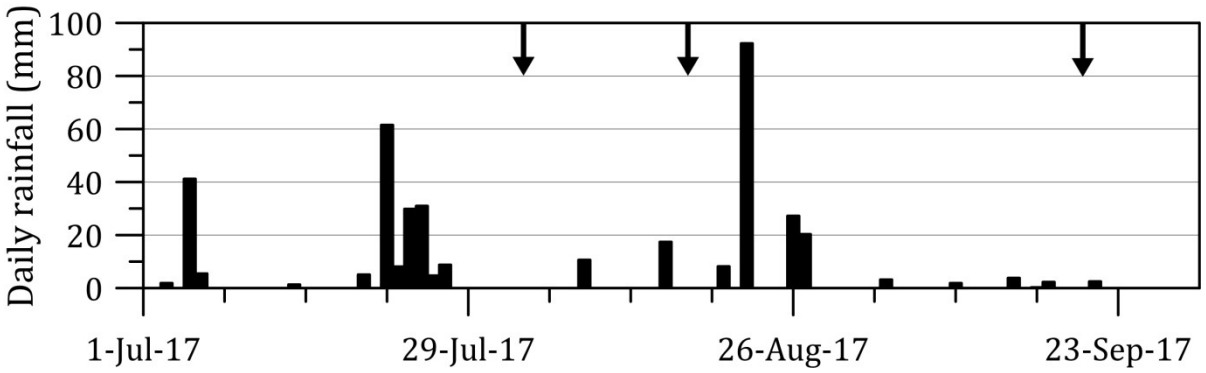
Daily rainfall (mm)
100
80
60
40
20
0
1-Jul-17
29-Jul-17
26-Aug-17
23-Sep-17

828 **Figure 4**

829

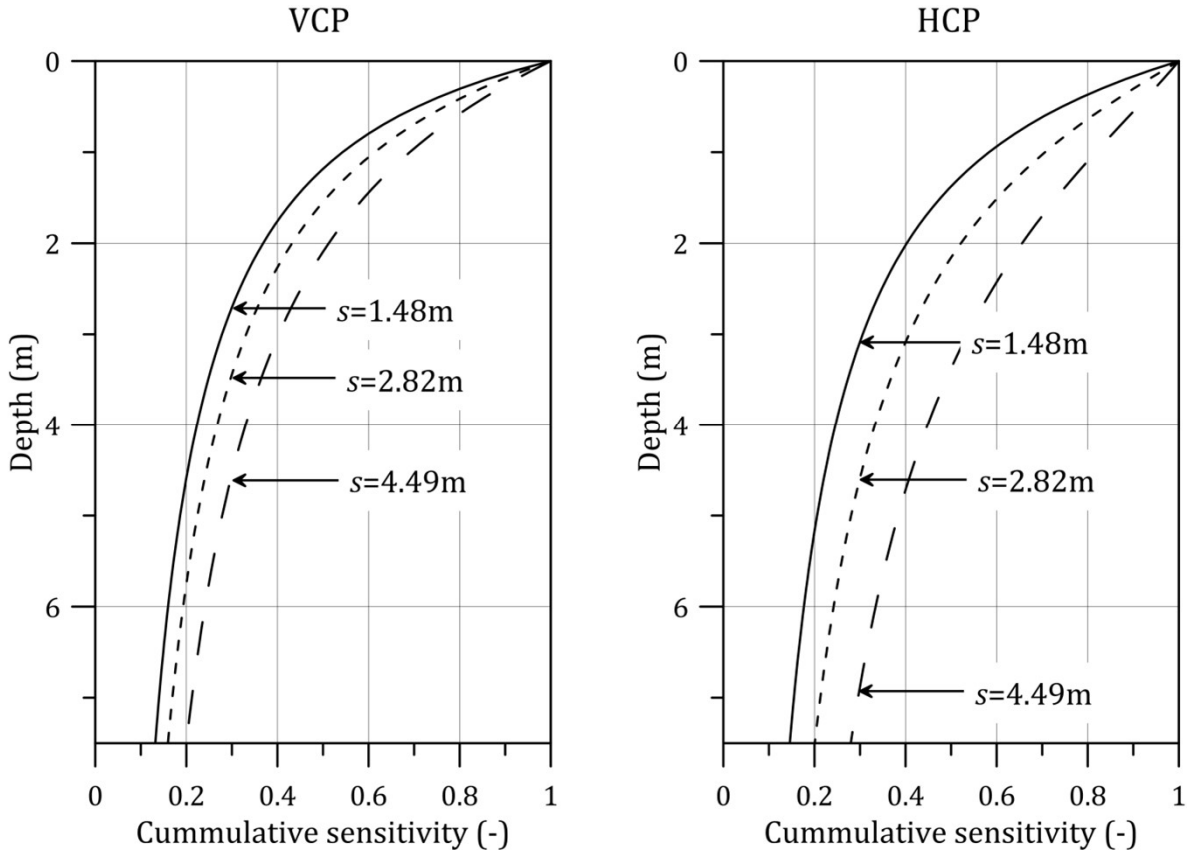

830

831

832 **Figure 5**

833

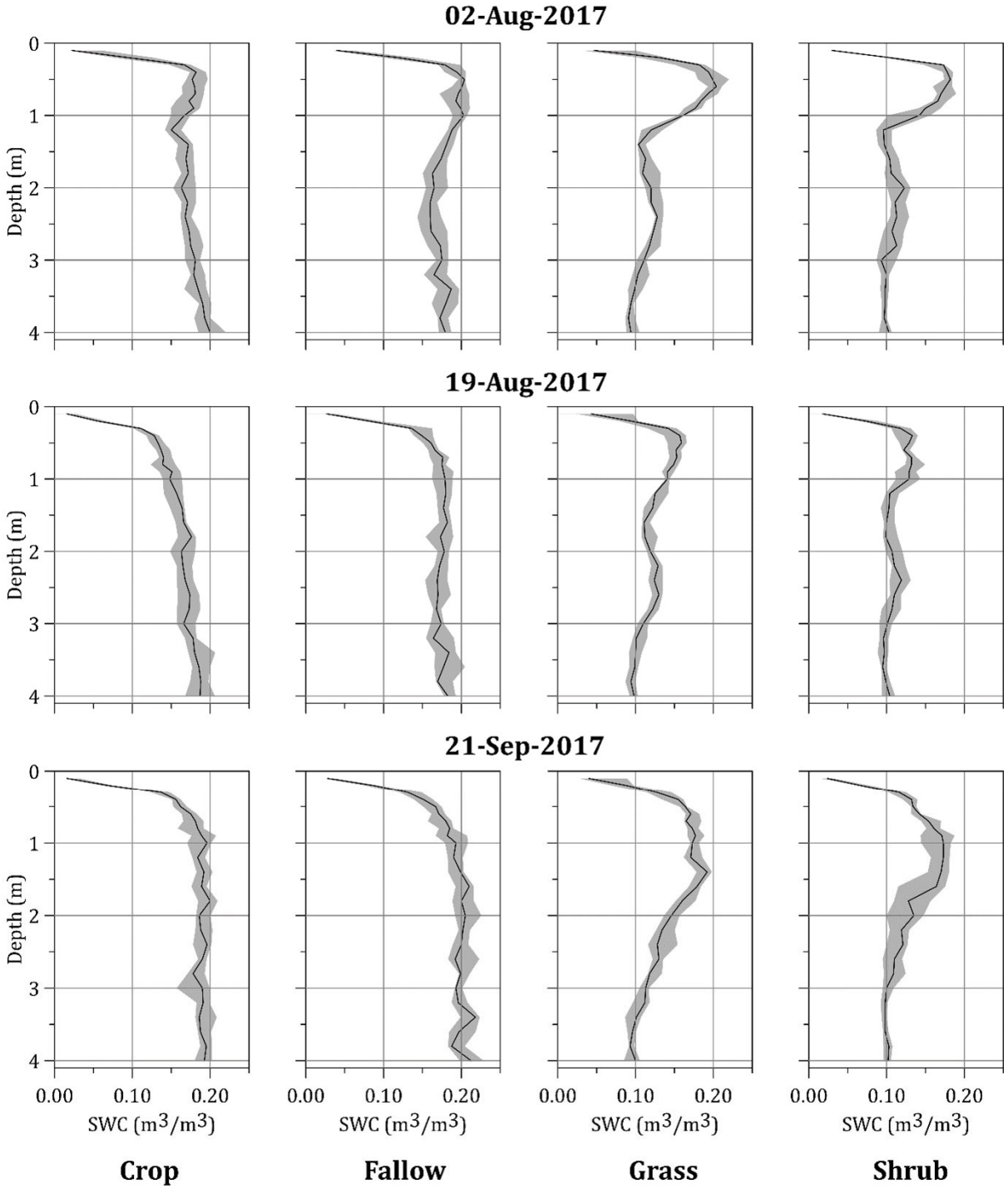

834

835

836

837

838 **Figure 6**

839

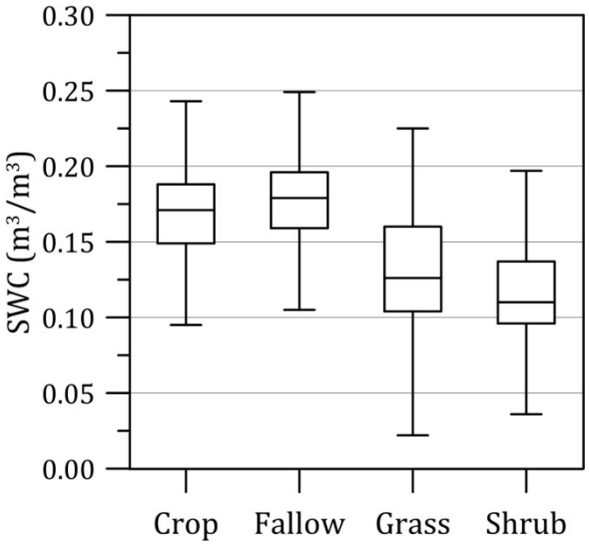

840

841

842

843 **Figure 7**

844

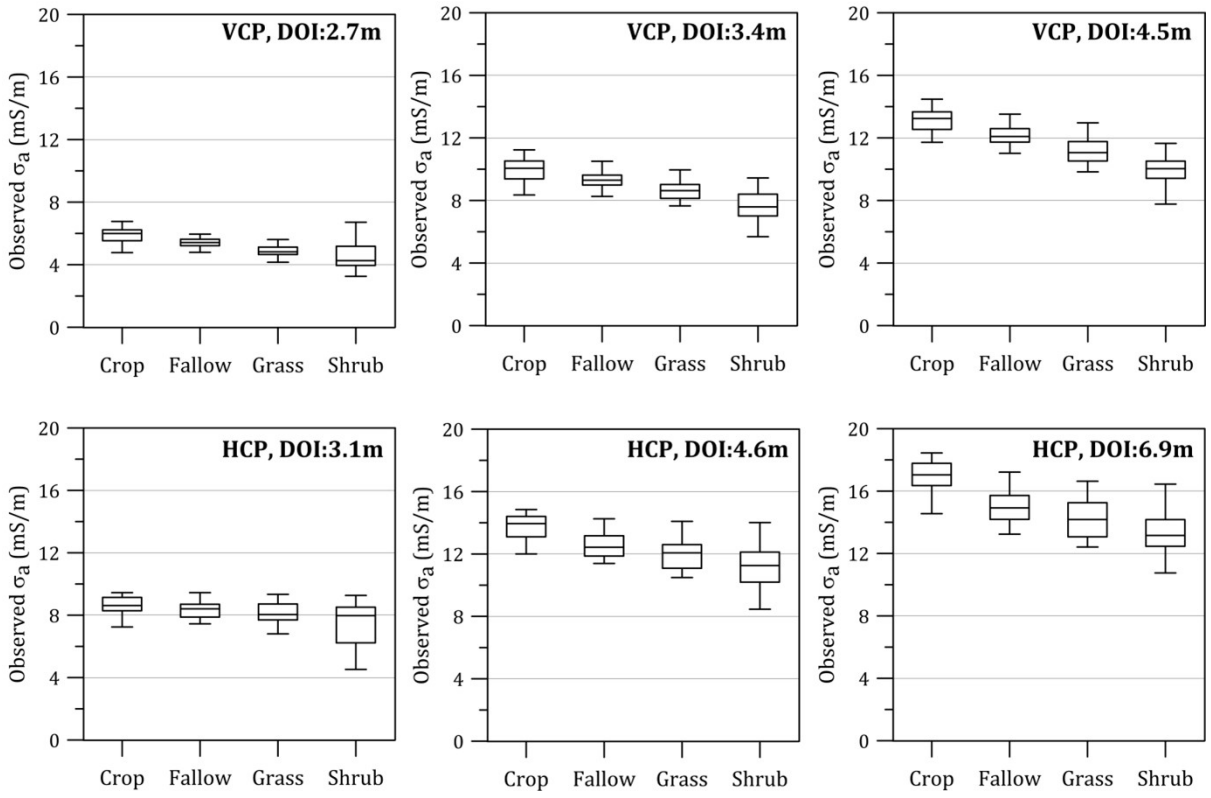

845

846

847

848 **Figure 8**

849

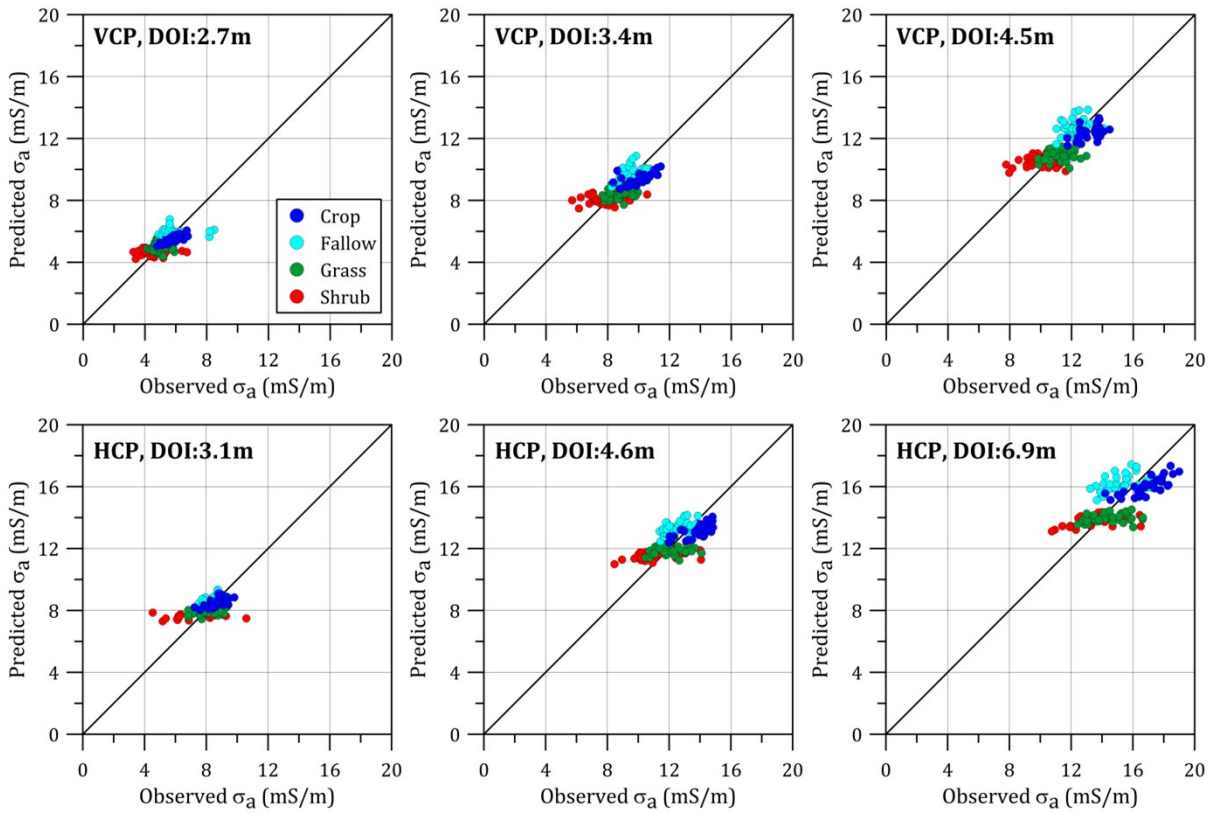

850

851

852 **Figure 9**

853

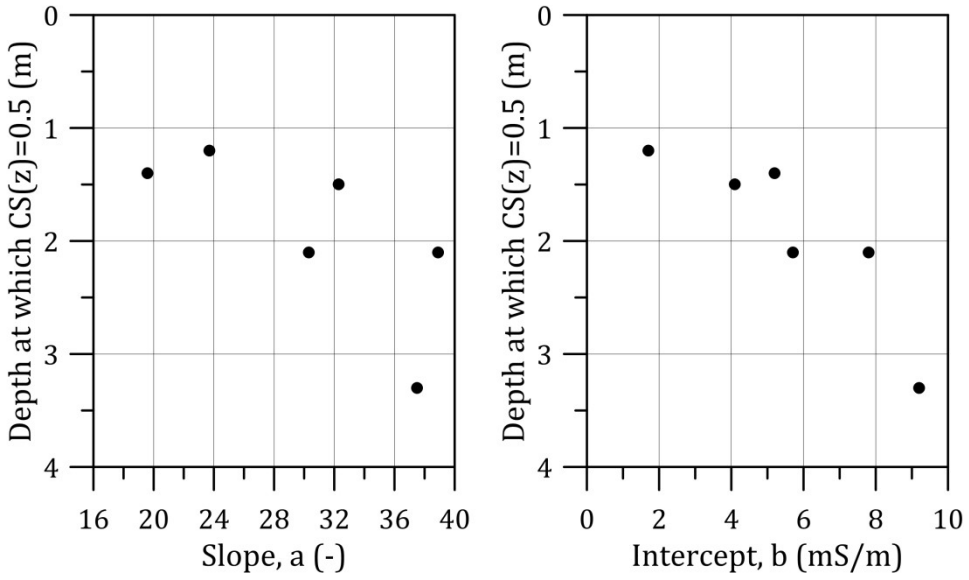

854

855

856 **Figure 10**

857

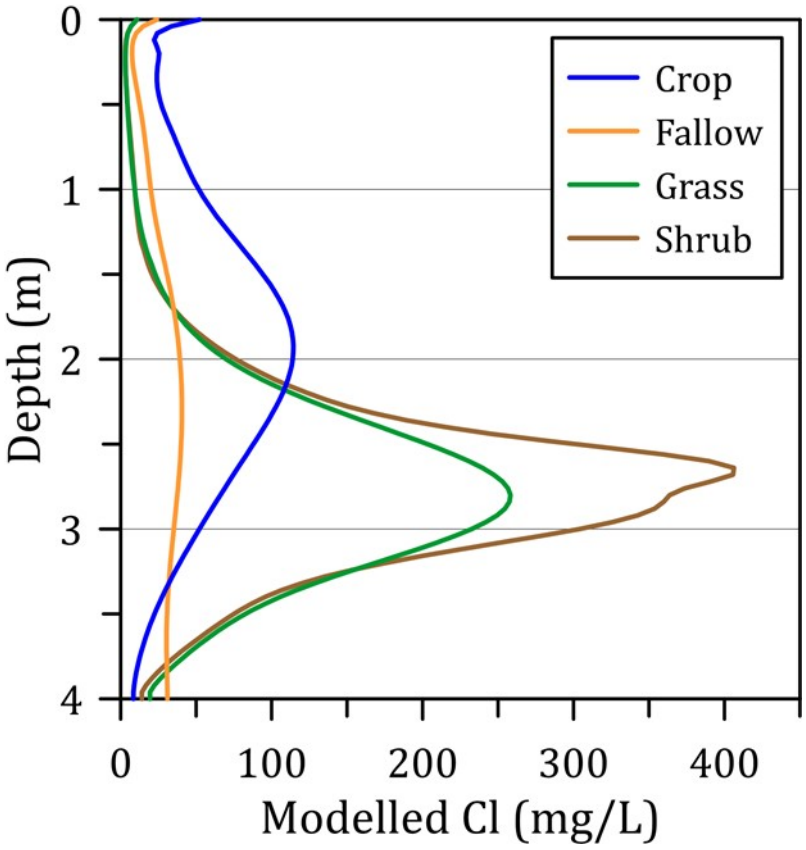

858